AD-A073 290 NAVAL RESEARCH LAB WASHINGTON DC F/G 20/14
MAXIMUM ENTROPY WAVENUMBER ANALYSIS.(U)
MAR 79 W R KING
UNCLASSIFIED NRL-8298 SBIE-AD-E000 311 NL

| OF |
AD
A073290

END
DATE
FILMED
10-79
DDC

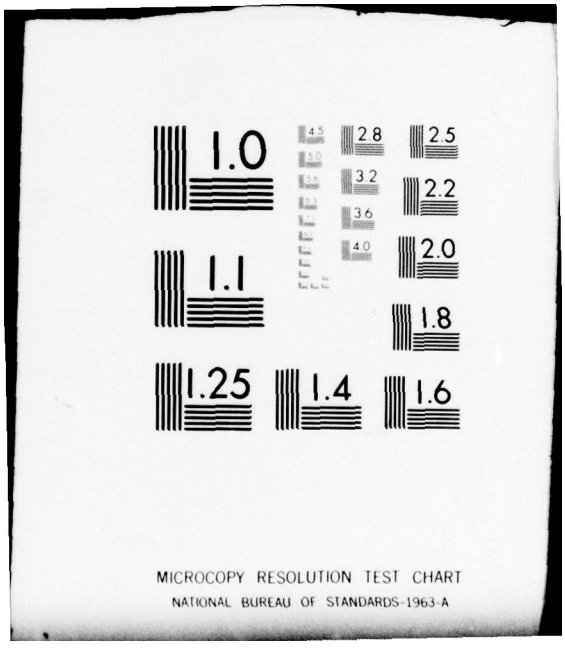
1.0
1.1
1.25
1.4
1.6
1.8
2.0
2.2
2.5
2.8
3.2
3.6
4.0
4.5
5.0
MICROCOPY RESOLUTION TEST CHART
NATIONAL BUREAU OF STANDARDS-1963-A

NRL Report 8298

Maximum Entropy Wavenumber Analysis

WILLIAM R. KING

Antenna Systems Staff
Radar Division

LEVEL II

March 20, 1979

NAVAL RESEARCH LABORATORY
Washington, D.C.

SECURITY CLASSIFICATION OF THIS PAGE (When Data Entered)

REPORT DOCUMENTATION PAGE		READ INSTRUCTIONS BEFORE COMPLETING FORM
1. REPORT NUMBER NRL Report 8298	2. GOVT ACCESSION NO.	3. RECIPIENT'S CATALOG NUMBER
4. TITLE (and Subtitle) MAXIMUM ENTROPY WAVENUMBER ANALYSIS		5. TYPE OF REPORT & PERIOD COVERED Interim report on a continuing NRL problem. 6. PERFORMING ORG. REPORT NUMBER
7. AUTHOR(s) William R. King		8. CONTRACT OR GRANT NUMBER(s) 53R12-46
9. PERFORMING ORGANIZATION NAME AND ADDRESS Naval Research Laboratory Washington, D.C. 20375		10. PROGRAM ELEMENT, PROJECT, TASK AREA & WORK UNIT NUMBERS RR021-05-41 61153N-21 R12-46.101
11. CONTROLLING OFFICE NAME AND ADDRESS Department of the Navy Office of Naval Research Arlington, VA 22217		12. REPORT DATE March 20, 1979 13. NUMBER OF PAGES 38
14. MONITORING AGENCY NAME & ADDRESS(if different from Controlling Office)		15. SECURITY CLASS. (of this report) UNCLASSIFIED 15a. DECLASSIFICATION/DOWNGRADING SCHEDULE

16. DISTRIBUTION STATEMENT (of this Report)

Approved for public release; distribution unlimited.

17. DISTRIBUTION STATEMENT (of the abstract entered in Block 20, if different from Report)

18. SUPPLEMENTARY NOTES

19. KEY WORDS (Continue on reverse side if necessary and identify by block number)

Antennas
Direction finding
Linear prediction filters
Maximum entropy processing
Spectral analysis

20. ABSTRACT (Continue on reverse side if necessary and identify by block number)

The maximum entropy spectral analysis (MESA) technique is applied to a linear spatial array of sensors to obtain wavenumber power spectra. The resultant wavenumber spectra are compared with conventional beamsteered antenna patterns using simulated signals mixed with Gaussian noise. The results indicate that the MESA technique, which is an all-pole model, may provide improved accuracy and improved spatial resolution of signals under varying signal-to-noise conditions. Some difficulties with MESA are noted, and further investigations are recommended.

DD FORM 1 JAN 73 1473 EDITION OF 1 NOV 65 IS OBSOLETE
S/N 0102-014-6601

SECURITY CLASSIFICATION OF THIS PAGE (When Data Entered)

CONTENTS

INTRODUCTION 1

THEORY 2

Power Spectra 2
Prediction Error Filter 5
Signal Simulation 6
Power Spectra Peaks 8

APPLICATIONS 10

MESA Examples 10
Single Signal 10
Two Closely Spaced Signals 11
Three Closely Spaced Signals 13
Pattern Averaging 14
Mixed Signals 17
Relative Signal Phase 20
Summary of Observed MESA Characteristics 20

OPTIMAL FILTER SIZE 23

CONCLUSIONS 25

REFERENCES 28

APPENDIX A — Wiener Prediction Filter 31

APPENDIX B — The Burg Technique 34

MAXIMUM ENTROPY WAVENUMBER ANALYSIS

Introduction

In recent years several methods have been introduced for estimating power spectra with considerably greater resolution than that provided by the conventional periodogram or the Blackman-Tukey windowed Fourier transform. Included among such techniques are maximum entropy spectral analysis (MESA) introduced by Burg [1], the autoregressive model (AR) spectral estimation introduced by Parzen [2], and the method of maximum likelihood as demonstrated by Capon [3]. Other methods offering high resolution, which utilize the Fourier transform, are described by Gerchburg [4] and Papoulis [5]. More recently, another spectral estimator has been introduced by Gray [6].

While none of these spectral estimators have been thoroughly investigated, there have been a few comparative examinations of some of the techniques conducted by Lacoss [7], Ulrych and Bishop [8], and Nuttall [9]. Of the comparisons investigated, in general, superior results are achieved by using the MESA method and the Burg technique [10] for estimating filter coefficients. The results are dramatic, and suggest that investigations of MESA and other high-resolution techniques be continued. Because of the high resolution and stability achieved with MESA in such initial investigations, these same properties are investigated further in this report where MESA is applied to the analysis of simulated, multichannel, spatial, phased-array data.

In the initial paper by Burg [1], where the principle of MESA is first suggested, the prediction error filter coefficients (which maximize the entropy) are specified with knowledge of the autocorrelation coefficients. However, in a second MESA paper, Burg [10] defined the prediction error filter coefficients as a function of a set of uniformly spaced data samples representative of the function of interest. In addition, Burg simplified the method for obtaining the filter coefficients with use of Levinson's recursion equations, and also noted in the second paper that the mean squared prediction errors may be minimized in both the forward and backward directions. These suggestions served to greatly facilitate the implementation of MESA and to significantly enhance the MESA properties. Taken together, the improvements suggested by Burg [10] are often referred to as the "Burg technique."

The concept of estimating power spectra by maximizing entropy appears unique in the history of science, yet the resultant expression for power spectra is identical to the representation of the all-pole method or autoregressive model (AR) introduced by Parzen [2]. In fact, van den Bos [11] and Kaveh and Cooper [12] have noted that MESA, as outlined by Burg [1], is equivalent to the AR method as described by Parzen. Therefore, it is of consequence to note that the different spectral estimates sometimes predicted with the two spectral estimation methods are not due to inherent model differences, but rather to

Manuscript submitted December 12, 1978.

the different methods used for evaluating the corresponding filter coefficients. With this realization, Ulrych and Bishop [8] conducted a comparative analysis of the Burg and Yule-Walker [13,14] techniques for evaluating MESA and AR filter coefficients. In a comparison of spectral estimation of harmonic components, Ulrych and Bishop showed that the MESA-Burg technique provided significantly greater resolution than did the AR-Yule-Walker technique. They noted that the resolution differences are not surprising when it is realized that the Yule-Walker technique has assumed a zero extension of the data samples, whereas the Burg technique contains no assumptions concerning the nonsampled data field.

Since the MESA and AR methods are most significant when processing short data sets, it is natural to use such methods for processing data collected with multielement electromagnetic antennas or acoustical arrays. Such methods may well make it possible to achieve high resolution by using unusually short antenna arrays. Consequently, in this report the resolution property of the MESA-Burg technique is examined as a function of input-data signal-to-noise ratios (S/η), number of antenna elements, numbers of signals, incident signal angle, relative signal amplitudes, and relative signal phase.

THEORY

Power Spectra

The maximum entropy power spectra (MESA), which was introduced by Burg [1], has been derived by Parzen [2] using statistical methods and by van den Bos [11] using an all-pole model representation. To further the understanding and acceptance of MESA, another derivation suggested by Blizard [15] is presented based upon discrete convolution filtering and minimization of the mean squared error.

Consider the one-step discrete convolution prediction filter described by Levinson [16] as follows:

$$\hat{x}_t = \sum_{n=1}^{N} a_n x_{t-n} , \tag{1}$$

where $\hat{x}_t$ is the prediction at time t of the function x_t which is sampled at time intervals $n(\Delta t)$. The N prediction coefficients are given by $a_1, a_2, \ldots a_N$. The error of the one-step prediction is ϵ_t, given by

$$\epsilon_t = x_t - \hat{x}_t ,$$

$$\epsilon_t = x_t - \sum_{n=1}^{N} a_n x_{t-n} . \tag{2}$$

The filtering and error analysis represented by Eqs. (1) and (2) is illustrated in Fig. 1, where filter coefficients a_n are multiplied by values of x_t sampled at time intervals $n(\Delta t)$, and the resultant multiplications are summed to obtain the prediction $\hat{x}_t$. The predicted signal $\hat{x}_t$ and the actual signal x_t are subsequently subtracted to obtain the prediction error ϵ_t.

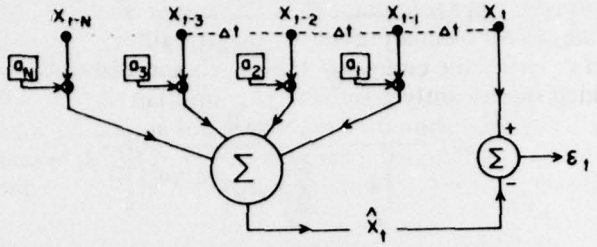

Fig. 1 — Prediction error filter

For convenience, the prediction error filter γ is introduced as follows:

$$\epsilon_t = \sum_{n=0}^{N} \gamma_n x_{t-n} , \tag{3}$$

where, in comparing Eq. (2) and (3), it is observed that

$$\gamma_0 = 1; \ \gamma_n = -a_n, \ n \geqslant 1.$$

Equation (3) is transformed to frequency space with the Fourier transform to obtain the following equation:

$$\xi_N(\omega) = X(\omega) \sum_{n=0}^{N} \gamma_n e^{i\omega n(\Delta t)} \tag{4}$$

where the Fourier transform of a function delayed $n(\Delta t)$ units is the exponential

$$e^{i\omega n(\Delta t)}$$

multiplied by the transformed function. The power spectra density function $P(\omega)$ is defined as

$$P(\omega) = X^2(\omega)/W,$$

where W is the bandwidth defined by the sampling interval Δt; i.e.,

$$W = \frac{1}{(\Delta t)} .$$

If the signal distribution function $X(\omega)$ is given by Eq. (4), the power spectra density function becomes

$$P(\omega) = \frac{\epsilon_N^2(\omega)/W}{\left| \sum_{n=0}^{N} \gamma_n e^{in(\Delta t)} \right|^2}, \tag{5}$$

$$P(\omega) = \frac{P_N/W}{\left| 1 + \sum_{n=1}^{N} \gamma_n e^{i\omega n(\Delta t)} \right|^2}, \tag{6}$$

where the error power $\xi_N^2(\omega)$ is represented by P_N. A requirement that the spectral error power $\xi_N^2(\omega)$ be a minimum results in P_N being independent of frequency as follows:

$$\frac{d\xi_N^2(\omega)}{d\omega} = 0,$$

$$\xi_N^2(\omega) = \text{constant}, \tag{7}$$

$$P_N = \text{constant}.$$

Then if P_N is a constant, the prediction error filter γ is a whitening filter, and P_N is also the mean of the total squared error as follows:

$$P_N = \xi_N^2(\omega),$$

$$P_N = \frac{1}{W} [\xi_N^2(\omega) W]. \tag{8}$$

The power spectra density function $P(\omega)$ given by Eq. (6) is the same MESA equation introduced by Burg [1] and later derived with detailed steps by Barnard [17].

The power spectra density (Eq. (6)) may also be expressed as a wavenumber power spectra density by

$$P(k) = \frac{P_N/K_{max}}{\left| 1 + \sum_{n=1}^{N} \gamma_n e^{ikn(\Delta x)} \right|^2}, \tag{9}$$

where the time (t) and frequency (f) variables have been transformed to space and wavenumber variables by using the following relations:

$$\omega = kc, \qquad \Delta t = \Delta x/c,$$

for

$k = (2\pi/\lambda)\cos\theta$,

λ = signal wavelength,

θ = signal angle of incidence,

c = signal velocity,

$K = 2\pi/\lambda$.

Prediction Error Filter

Utilization of the MESA power spectra equation (Eqs. (6) and (9)) requires that the prediction error coefficients γ_n and the mean error power P_N be known. These unknown parameters may be specified by minimizing the average time-dependent prediction error power $\overline{\epsilon^2}$. The resulting $N + 1$ equations, which are derived in Appendix A, are presented in a matrix formulation as

$$\begin{bmatrix} r_0 & r_1 & r_2 & r_3 \cdots r_N \\ r_1^* & r_0 & r_1 & r_2 \cdots r_{N-1} \\ r_2^* & r_1^* & r_0 & r_1 \cdots r_{N-2} \\ & & & \\ \cdot & & & \\ \cdot & & & \\ \cdot & & & \\ r_N^* & r_{N-1}^* & r_{N-2}^* & r_{N-3} \cdots r_0 \end{bmatrix} \cdot \begin{bmatrix} \gamma_0 \\ \gamma_1 \\ \gamma_2 \\ \\ \cdot \\ \cdot \\ \cdot \\ \gamma_N \end{bmatrix} = \begin{bmatrix} P_N \\ 0 \\ 0 \\ \\ \cdot \\ \cdot \\ \cdot \\ 0 \end{bmatrix}, \tag{10}$$

where it is known that $\gamma_0 = 1$ and it is assumed that the autocorrelation coefficients r_i (with lag $i\Delta t$) are known for N lags.

The autocorrelation coefficients have the following definition:

$$r_n = \lim_{M\to\infty} \frac{1}{2M + 1} \sum_{k=-M}^{M} X_k X_{k-n}^* . \tag{11}$$

But for a finite data set, the autocorrelation coefficients may be computed by approximating Eq. (11) with a finite summation over M data samples.

For large-sized filters (N large), solution of the $N + 1$ equations given by Eq. (10) becomes very tedious. Fortunately, Burg [10] demonstrated a more expeditious method for specifying the unknown prediction error coefficients which appear in Eqs. (6) and (9). He noted that the unknown parameters P_N and γ_n^N may be evaluated with repeated use of Levinson's recursion relations

$$P_{N+1} = P_N \left[1 - (\gamma_{N+1}^{N+1})^2\right], \tag{12}$$

$$\gamma_n^{N+1} = \gamma_n^N + \gamma_{N+1}^{N+1} \left(\gamma_{N-n+2}^N\right)^*, \tag{13}$$

for

$$P_1 = r_0^2,$$

$$\gamma_0^{N+1} = 1,$$

$$N \geqslant 1,$$

and with knowledge of γ_{N+1}^{N+1}, which is shown in Appendix B to have the following representation:

$$\gamma_{N+1}^{N+1} = \frac{2 \sum_{k=1}^{M-N-1} \left(\beta_k^N\right)^* \alpha_{k+n}^N}{\sum_{k=1}^{M-N-1} \left[\left(\beta_k^N\right)^2 + \left(\alpha_{k+N}^N\right)^2\right]}, \tag{14}$$

where the forward prediction error is α_k^N and the backward prediction error is β_k^N. The three equations, Eq. (12), (13), and (14), comprise the Burg technique as originally demonstrated by Burg [10] and later generalized in detail by Anderson [18] and Barnard [17].

The remainder of this report is concerned with the properties exhibited by the MESA wavenumber power spectra equation (Eq. (9)) when evaluated using the Burg technique given by Eqs. (12-14).

Signal Simulation

Resolution properties of the MESA-Burg technique are examined by using simulated antenna data. Input signals to a linear (line), multielement, phased-array antenna are assumed to be plane waves mixed with white Gaussian noise. The multichannel signals are preprocessed with narrowband filtering and channel delays which serve to "direct" (or steer) the antenna in the direction of the incident plane-wave signal. The preprocessing methods are illustrated in Fig. 2 where the nth channel is depicted as delayed $(n - 1)\ \Delta t$ seconds for

$$\Delta t = \Delta x \sin(\theta)/c,$$

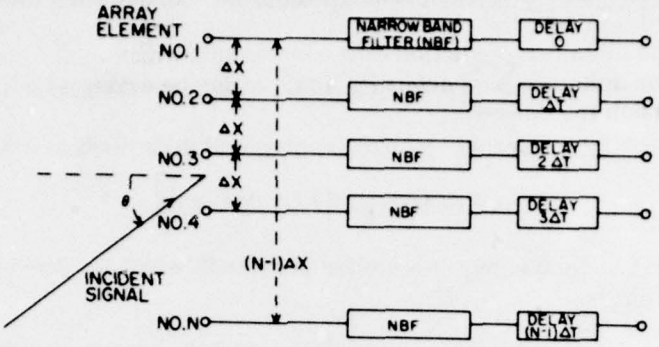

Fig. 2 — Preprocessing of a linear phased array

where c is the velocity of the incident signal, Δx is the antenna element spacing, and θ is the look angle of the steered array measured relative to the normal to the array.

The signal $x_n(\theta)$ incident to the nth antenna element is represented as

$$x_n(\theta) = A \exp[i\Omega_n(\theta)] + Q_n \exp(i2\pi q_n), \tag{15}$$

where A is the signal amplitude, $\Omega_n(\theta)$ is the signal total phase, and Q_n is a random number representative of Gaussian noise. The amplitudes A and Q_n are relative, and are determined by a Gaussian distribution with variance σ^2 and a specified signal-to-noise ratio as follows:

$$\frac{S}{\eta} = \frac{A^2}{2\sigma^2}, \tag{16}$$

$$q_n = e^{-Q_n^2/2\sigma^2}, \tag{17}$$

where S/η is the input signal-to-noise power ratio, σ^2 is the average noise power, and q_n is a random number between 0 and 1.0 obtained by using a "white" random number generator.

The signal phase $\Omega_n(\theta)$ has three components as follows:

$$\Omega_n(\theta) = 2\pi i[n-1][\Delta x/\lambda][\sin(\theta) - \sin(\theta_s)] - \phi, \tag{18}$$

where θ is the array look angle, θ_s is the angle of the incident signal relative to the normal to the array, ϕ is the incident signal initial phase with values between 0 and 2π, and λ is the signal wavelength given by

$$\lambda = c/f.$$

For all signals analyzed in this report, the ratio $\Delta x/\lambda$ has the value 0.5; i.e.,

$$\Delta x/\lambda = 0.5.$$

In conventional beamforming all N antenna elements are summed such that the total $X(\theta)$ is

$$X(\theta) = \sum_{n=1}^{N} \{A \exp[i\Omega_n(\theta)] + Q_n \exp(i2\pi q_n)\}, \tag{19}$$

and the conventional antenna power pattern is computed in decibels as follows:

$$\text{dB} = 10 \log [X^2(\theta)/X^2(\theta_s)]. \tag{20}$$

However, the MESA technique requires multichannel data which are given by Eqs. (15) and (18).

Conventional antenna patterns are compared with MESA patterns whenever such comparisons are considered worthwhile. It is specifically noted that the S/η is defined at the antenna element and is the same for each antenna element. Consequently, the S/η does not include the conventional antenna gain factor.

Power Spectra Peaks

The wavenumber power spectrum given by Eq. (9) may be expressed by

$$P(k) = \frac{P_N/K}{\Gamma^2(k)}, \tag{21}$$

where

$$\Gamma(k) = \left| 1 + \sum_{n=1}^{N} \gamma_n e^{ikn(\Delta x)} \right|$$

or

$$\Gamma(k) = \left| \sum_{n=0}^{N} \gamma_n e^{ikn(\Delta x)} \right|$$

for

$\gamma_0 = 1.0$,

$k = K \sin\theta$,

$K = 2\pi/\lambda$.

Spectral peaks of $P(k)$, which occur at minimal values of $\Gamma(k)$, may be located by solving for the roots of the function $\Gamma(z)$ in the complex z-plane as follows.

Consider a polynomial $\Gamma(z)$ defined as

$$\Gamma(z) = \sum_{n=0}^{N} \gamma_n z^n , \tag{22}$$

where

$$\begin{aligned} z &= |z| e^{i\phi} , \\ \phi &= k\, n\, (\Delta x), \\ \phi &= \pi n \sin\theta \text{ for } (\Delta x) = \lambda/2. \end{aligned} \tag{23}$$

The polynomial $\Gamma(z)$ (of order N) may also be expressed as a function of the N complex roots as follows:

$$\Gamma(z) = |(z - z_1)(z - z_2) \ldots (z - z_N)| , \tag{24}$$

where $z_1, z_2, \ldots z_N$ are the N roots located in the complex z-plane. The significance of $\Gamma(z)$ becomes obvious from the observation that the function of interest $\Gamma(k)$ is actually the polynomial $\Gamma(z)$ on the unit circle, i.e.,

$$\Gamma(k) = \Gamma(z) \text{ for } |z| = 1.0.$$

Consequently, $\Gamma(k)$ has a polynomial representation in the z-plane as follows:

$$\Gamma(k) = |(e^{i\phi} - z_1)(e^{i\phi} - z_2) \ldots (e^{i\phi} - z_N)|, \tag{25}$$

where it is recalled that ϕ and k are functionally related according to Eq. (23). The product terms of $\Gamma(k)$ in Eq. (25) are the complex vectors $(e^{i\phi} - z_j)$ which are shown constructed in the z-plane diagram of Fig. 3. In accordance with Eq. (25), the minimal values of $\Gamma(k)$ occur at minimal values of the complex vectors $(e^{i\phi} - z_j)$. And as observed in Fig. 3 the complex vectors $(e^{i\phi} - z_j)$ are minimal for ϕ corresponding to ϕ_j, the argument of the complex roots z_j; i.e.,

$$\phi = \phi_j \text{ where } \phi_j = \arg(z_j).$$

Consequently, stronger spectral peaks, which occur for smaller values of $\Gamma(k)$, occur for roots z_j lying closer to the unit circle. And as noted by Burg (in private communication), all roots of Eq. (22) lie outside the unit circle.

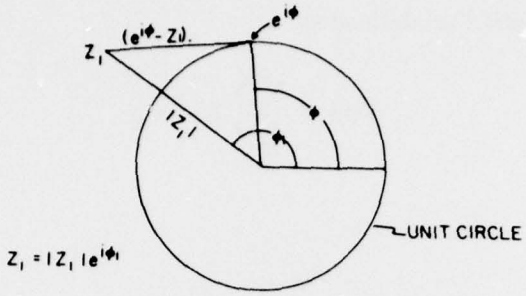

Fig. 3 — Z-plane with root Z_1

APPLICATIONS

MESA Examples

Several examples of MESA antenna patterns are computed in order to demonstrate MESA characteristics. Antenna patterns are computed for linear antennas containing 8 or 16 elements spaced at half-wavelength intervals, and for various signal-to-noise ratios. Snapshot-type antenna patterns are presented to demonstrate the explicit MESA characteristics. A MESA snapshot pattern is a MESA antenna pattern computed by using N discrete data points representing spatial data collected at one instant of time. In some examples several MESA snapshot patterns may be averaged to obtain one single representative stable antenna pattern. Some type of averaging is usually recommended when MESA is applied to actual data. Usually, it is better to use a time average of either the input autocorrelation matrix, the prediction error, or the prediction filter coefficients. However, in this demonstration of MESA characteristics it is convenient to obtain pattern stability with the averaging of snapshot patterns (or postprocessor integration).

The MESA algorithm, used to compute the examples in this report, utilizes complex number arithmetic throughout, so that the input-signal and noise data may have a complex representation. As a result, the prediction filter coefficients computed by the algorithm are complex coefficients.

Each example MESA antenna pattern is computed for a noise field identified by a "seed" number required of the random number generator. The exhibited antenna patterns may be duplicated only with use of the particular seed number (IR) that is identified in each example.

Single Signal

A MESA snapshot antenna pattern is shown in Fig. 4 for a single signal incident to an 8-element antenna at 0° (broadside to the antenna) with a S/η of 0 dB. In this particular snapshot pattern, which is computed by using a 6-point prediction filter (N=6), the signal peak is about 10.5 dB above the largest noise peak. There are N peaks in a MESA snapshot which is computed for an N-point prediction filter, and in Fig. 4 there are five prominent

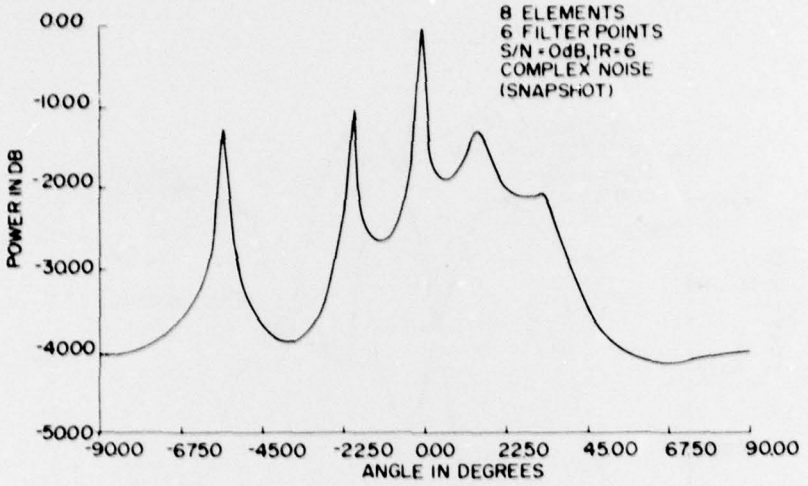

Fig. 4 — One signal at 0° (low S/η)

peaks and one small peak located at 90°. The noise peaks would be distributed differently in a MESA snapshot computed for a subsequent noise field. The noise field used in computing the MESA snapshot pattern consists of eight random (white) complex numbers representative of receiver noise.

The same noise data of Fig. 4 are summed with a signal at 0° having a S/η of 10 dB to obtain the MESA snapshot pattern shown in Fig. 5. Since the noise data are identical in Figs. 4 and 5, the noise peaks have the same location in both examples, but the noise peaks of Fig. 5 are further suppressed (both snapshot patterns are normalized at the signal peak).

A conventional antenna pattern is also shown in Fig. 5 for comparison purposes, where the conventional pattern is observed to have a beamwidth of about 15° at the half-power (3-dB) points on the main lobe. The width of the MESA signal peak in Fig. 5 is so narrow as not to be measurable on the plotted pattern. Since points are computed at 1° intervals, it can only be stated that the MESA signal peak is down by 16 dB at the 1° intervals on either side of the peak occurring at 0°. In the particular MESA snapshot illustrated in Fig. 5 there is also considerable reduction in side-peak levels in comparison with the conventional pattern. However, side-peak levels vary significantly in subsequent MESA snapshots. Consistent side-peak levels are possible only with some type of preprocessor or postprocessor averaging.

Two Closely Spaced Signals

Two signals incident at angles of −4° and 4° are readily identified in the MESA snapshot shown in Fig. 6 for a complex noise and a S/η of 13 dB, each signal, each element. The MESA snapshot is computed for an 8-element antenna and a 6-point prediction filter, which is denoted by the six peaks appearing in Fig. 6. Since particular snapshot patterns are not necessarily repetitive over a finite time interval, a more representative MESA antenna pattern is obtained by averaging 20 such snapshot patterns, as shown in Fig. 7.

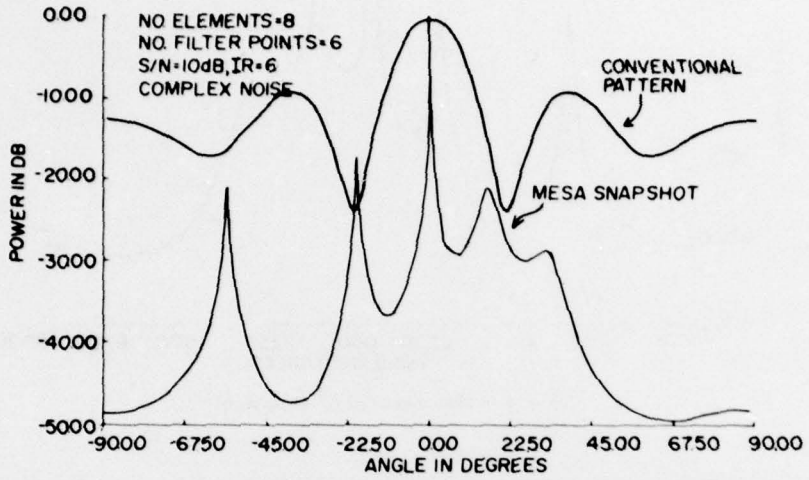

Fig. 5 — One signal at 0°

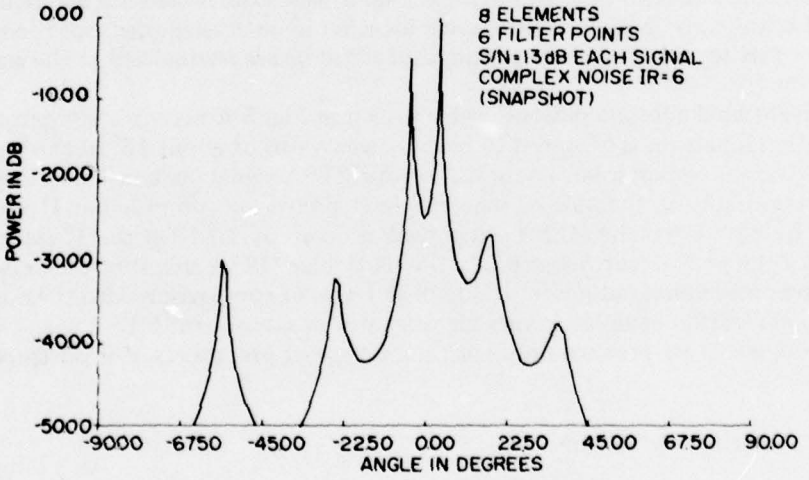

Fig. 6 — Two signals at −4° and 4°

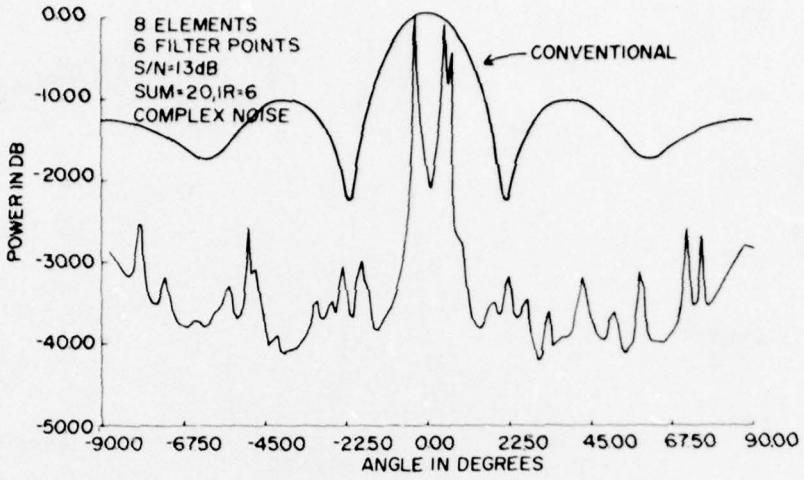

Fig. 7 — Two signals at -4° and 4° (summed patterns)

While the two signals are resolved in the averaged MESA pattern of Fig. 7, the resolution of the averaged pattern is not as favorable as the particular MESA snapshot illustrated in Fig. 6. However, the two signals are not resolved by the conventional antenna pattern (also shown in Fig. 7), which is computed as the sum of two conventional patterns obtained by "steering" the array in the directions of the two signals. It is known that the resolution of a conventional antenna pattern is given approximately by the function R as follows:

$$R \approx \text{arc sin } (\lambda/L),$$

where λ is the signal wavelength and L is the array length. For an 8-element antenna having half-wavelength element spacing,

$$R \approx \text{are sin } (2/7)$$

$$\approx 16.6 \text{ degrees.}$$

For the parameters illustrated in Fig. 7, the resolution of MESA is at least a factor of two better than the conventional pattern.

Three Closely Spaced Signals

A MESA snapshot is shown in Fig. 8, computed for three signals incident at angles of -7°, 0°, and 7°, with each signal having a S/η of 40 dB, each element. The MESA snapshot, computed for a 6-point filter and omnidirectional noise, has four equally strong peaks and two low-level side peaks. It is apparent that the central signal at 0° is represented by two split peaks on either side of the true signal location. The MESA snapshot pattern depicts "peak splitting," which is sometimes observed in MESA snapshots at the larger filter sizes, but is encountered less frequently in averaged MESA antenna patterns.

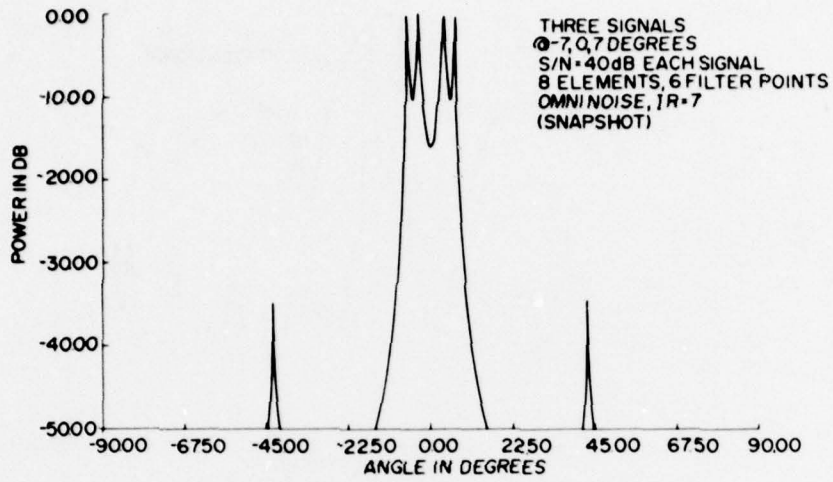

Fig. 8 — Splitting with three signals

For example, an average of 20 MESA snapshots, including the one shown in Fig. 8 (since the same seed number is used), is shown in Fig. 9 to illustrate that pattern averaging serves to enhance MESA stability. In comparing Figs. 8 and 9, it is observed that even though stability is enhanced by averaging, peak widths are increased.

Further examples of three resolved signals are shown in Figs. 10 and 11, where the effect of increased S/η is depicted. In Fig. 10 the noise field is omnidirectional and the three peaks are predicted within 0.5° of the correct incident angles. Also, MESA patterns computed with omnidirectional noise have an observed symmetry in peak location, whereas MESA patterns computed for complex noise distributions do not exhibit such symmetry as demonstrated by the snapshot patterns in Fig. 11.

The MESA snapshot patterns in Figs. 10 and 11 do indicate that resolution is improved and side-peak levels are reduced with increased S/η. These benefits are demonstrated in Figs. 10 and 11 for a S/η increase of 20 dB. The two examples also illustrate that omnidirectional noise does not affect the accuracy of peak location, but complex noise may cause such inaccuracies or distortions. It appears that complex noise (receiver noise) is a more troublesome noise than the spatial omnidirectional noise field.

Pattern Averaging

While it has been demonstrated that pattern averaging provides stability to MESA antenna patterns, averaging also serves to broaden peak widths in comparison to MESA snapshot patterns. The averaged pattern of Fig. 9 demonstrated MESA stability for omnidirectional noise.

Another benefit of pattern averaging for omnidirectional noise is illustrated in Fig. 12, where side-peak levels have been substantially reduced. In the example, a MESA snapshot

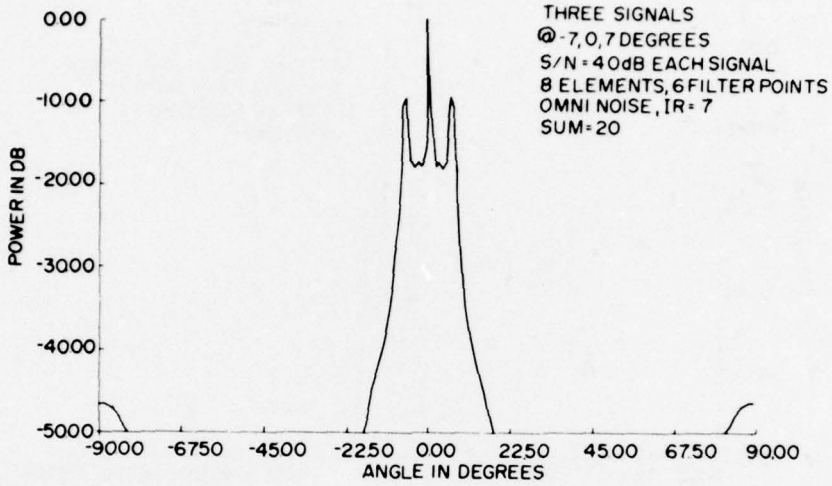

Fig. 9 — Three signals (summed patterns)

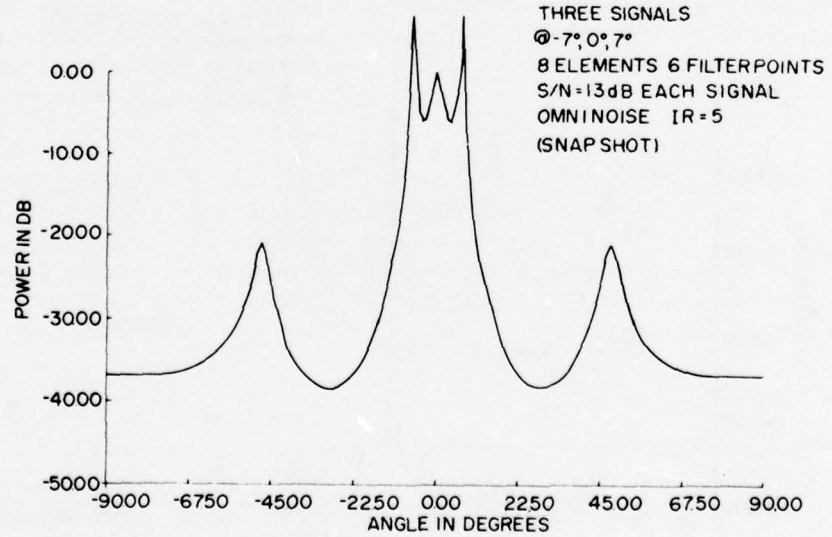

Fig. 10 — Three signals (snapshot)

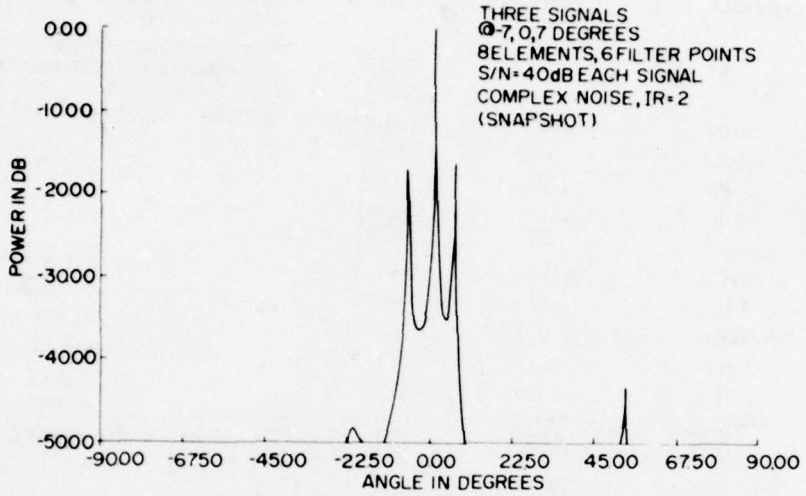

Fig. 11 — Three signals (complex noise)

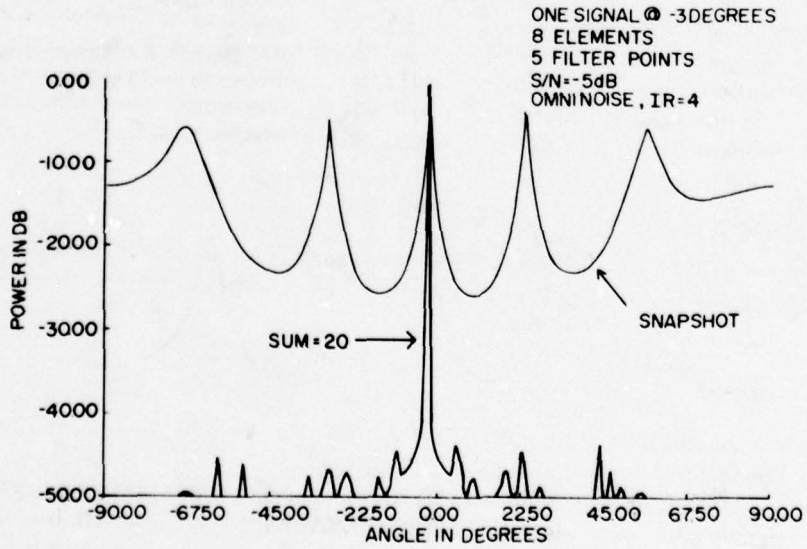

Fig. 12 — Signal at -3°

pattern is shown for one signal incident at -3° to an 8-element antenna. From the number of peaks in the snapshot it is noted that a 5-point prediction filter is used. An average of 20 such snapshot patterns indicates a substantial reduction in side-peak levels that is much greater than anticipated from the gain due only to a uniform distribution of side peaks in the 20 MESA snapshots. For in an ordinary summation of snapshots such a gain is only

$$10 \log (M),$$

where M is the number of patterns summed. Consequently, it is anticipated that side-peak levels may be reduced by only 13 dB in an average of 20 MESA snapshots. No explanation is suggested for the gain that is apparent in Fig. 12, but if the apparent gain is real, then signal detection may be improved substantially with pattern averaging.

The effect of averaging MESA snapshots computed for complex noise is demonstrated in Figs. 13 and 14. A MESA snapshot of one signal incident at -3° is illustrated for a 7-point filter in Fig. 13 where the S/η is 0 dB. It is apparent from the averaged MESA pattern shown in Fig. 14 that signal detection in complex noise is improved with averaged MESA patterns, but the amount of improvement is not demonstrated by a single MESA pattern. However, detection performance may be measured with a large collection of such patterns by constructing a set of ROC (receiver operating characteristic) curves that illustrate the probability of detection for specific false alarm rates. In the particular example of Fig. 14, there is an apparent gain of about 5 dB in S/η level for a zero false alarm rate. The gain appears even more substantial in some following examples.

The S/η gain that is apparent with the previous examples of averaged MESA patterns appears to indicate that the gain is substantially greater with MESA patterns computed for omnidirectional noise. One obvious reason for this discrepancy is observed in Figs. 10 and 11, where complex noise affects the accuracy of the location of signal peaks, thereby reducing the effect of pattern summation. There is little or no observable effect upon peak location with omnidirectional noise. Consequently, the signal peaks summed in patterns for omnidirectional noise remain sharply defined, whereas the signal peaks summed in patterns for complex noise are distorted and broadened and show only a moderate S/η gain due to pattern averaging.

To recount the benefits attributable to pattern averaging, the examples presented indicate that averaging of a sufficient number (maybe 20 or so) of MESA snapshot antenna patterns provides pattern stability, helps to eliminate peak splitting, and may provide a significant gain in signal detection.

Mixed Signals

A MESA snapshot antenna pattern is shown in Fig. 15 for a collection of five signals in complex noise having S/η's of 0, 10, and 20 dB as indicated in the illustration. The example of Fig. 15 is computed for an antenna with 16 elements and a 13-point prediction filter. Only two of the signals are clearly identified in the MESA snapshot of Fig. 15, but all five signals are readily and accurately detected in an average of 20 such MESA snapshots as shown in Fig. 16. Signal detection is considerably improved in the averaged MESA pattern which consists of signals mixed with complex noise. It is apparent that the particular set of complex noise samples (IR = 5) has not adversely affected signal-peak location accuracy as was noted in the previous examples of Figs. 11 and 14.

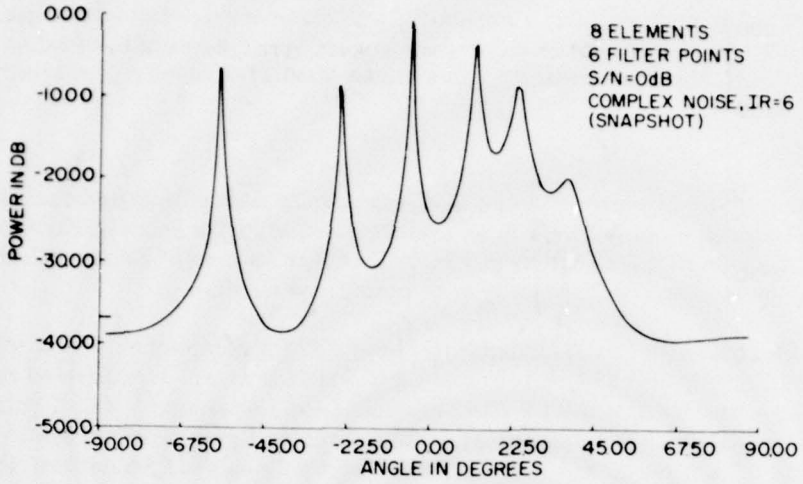

Fig. 13 — Signal at -3° (snapshot)

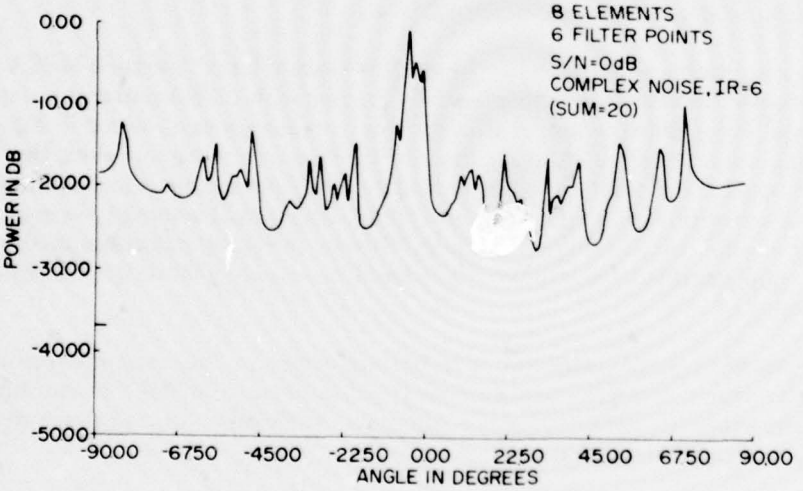

Fig. 14 — Signal at -3° (summed patterns)

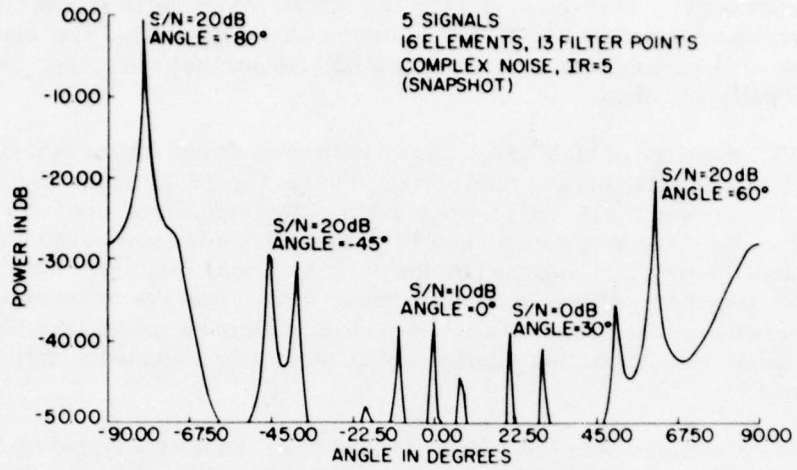

Fig. 15 — Five signals (snapshot)

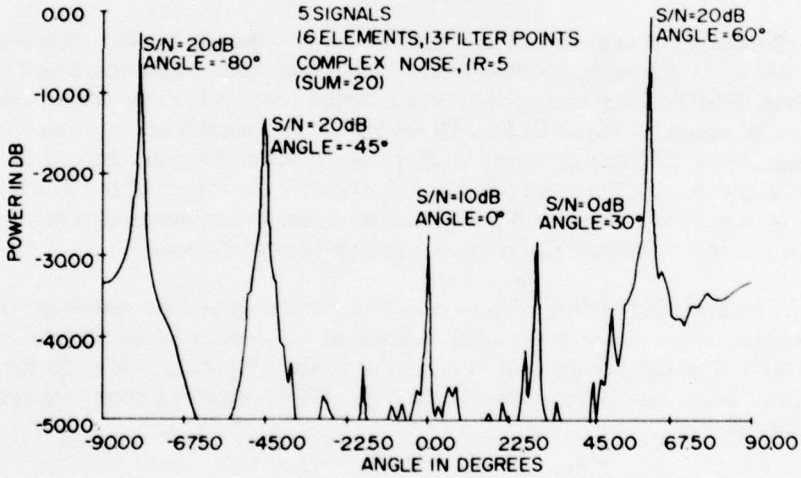

Fig. 16 -- Five signals (summed patterns)

Relative Signal Phase

It has been noted by Fougere, et al. [19] that signals having initial phases other than zero are not accurately predicted by MESA. In particular, Fougere noted that signals with an initial phase of $\pi/4$ are most troublesome for MESA, as peak splitting is apparently most severe for this particular phase.

In Fig. 17, an average of 20 MESA snapshot patterns is shown for the same five signals and noise and the same antenna and filter size depicted in Fig. 16. However, the signal incident at 60° has a phase of $\pi/4$ (45°) relative to the other four signals, all of which have zero initial phase. In comparing Figs. 16 and 17 it is noted that the two signals located at 30° and 60° are considerably broadened by the phase shift, which suggests that some of the summed MESA snapshots either contain inaccurately located peaks or suffer some peak splitting at these two signal locations. Whatever occurs, pattern averaging has again served to maintain pattern stability so that signal peaks are accurately predicted even though somewhat broadened.

In a further examination of the effects of signal phase, another averaged MESA antenna pattern is shown in Fig. 18 for the same signals and noise and parameters of the two preceding examples. The exception is that the signal incident at 60° has a relative phase of π (180°). There is evidence of severe peak splitting at the wider angle signals. It appears that a signal phase of π is most troublesome for MESA and is responsible for severe loss in accuracy and peak distortion.

Phase distortion effects are examined further for two closely spaced signals separated by 6° with a S/η of 20 dB each, and detected with an 8-element antenna using a 6-point prediction filter. The resulting averaged MESA antenna pattern for the two signals, both having zero initial phase, is shown in Fig. 19 where the two signals are separated by a shallow null of only a few dB. The averaged MESA pattern for one signal (the one at +3°) having an initial phase of $\pi/2$ is shown in Fig. 20. Clearly, the effect of the $\pi/2$ relative (and initial) phase is to shift the two signal peaks further apart and to enhance resolution at the loss of accuracy. Also, the signal peaks appear somewhat broadened.

In Fig. 21 an averaged MESA pattern is shown for the same two signals in the two previous examples, but with the one signal incident at +3° having an initial (and relative) phase of π (180°). The pattern distortion is similar to that depicted in Fig. 20 for a relative phase of $\pi/2$, but is not nearly so severe. Distortion effects are also minor (similar to Fig. 21) for a phase shift of $\pi/4$.

Summary of Observed MESA Characteristics

The illustrations of MESA antenna patterns show that these patterns have substantially reduced peak widths and consequently have better resolution than conventional antenna patterns. Also, signal detection with MESA appears to be improved over signal detection with conventional patterns. Such improvement is indicated by the substantial reduction in side (noise) peak levels achieved with postprocessor integration (pattern averaging).

Multiple signals of varying power levels may be accurately predicted with MESA, although the number of antenna elements must be greater than twice the number of signals to be detected.

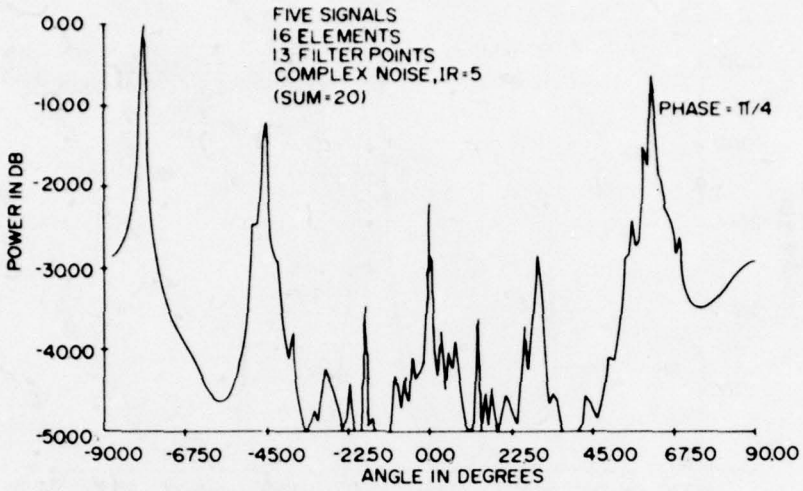

Fig. 17 — Five signals (phase at 60° is $\pi/4$)

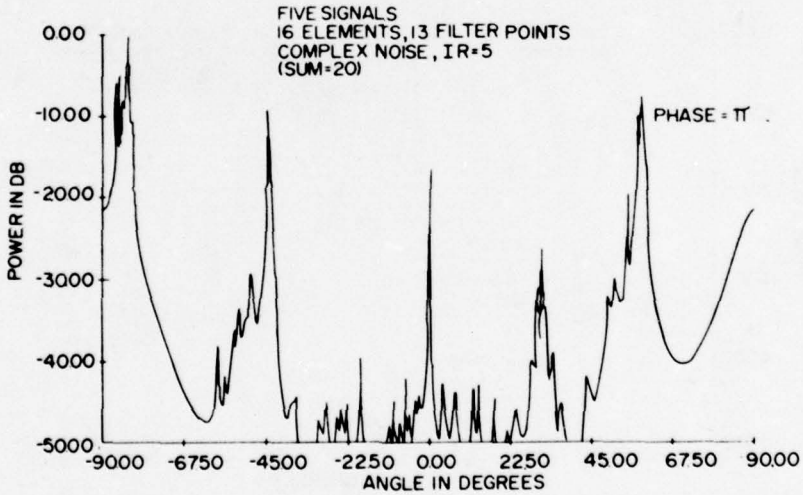

Fig. 18 — Five signals (phase at 60° is π)

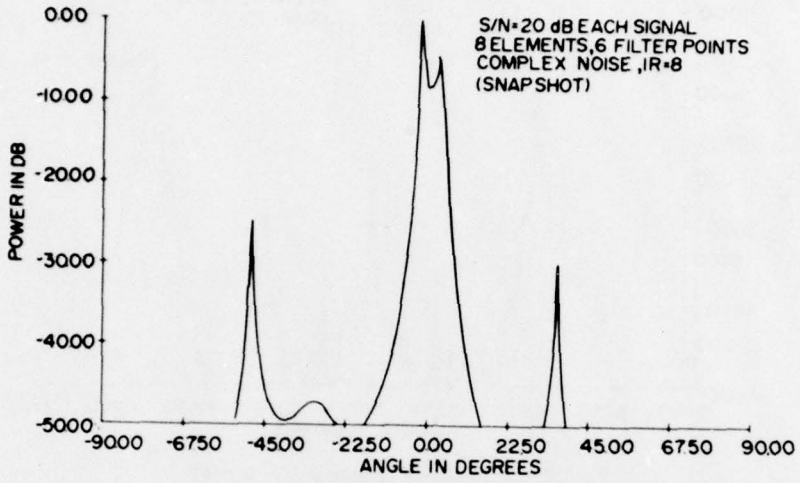

Fig. 19 — Two signals at -3° and 3°

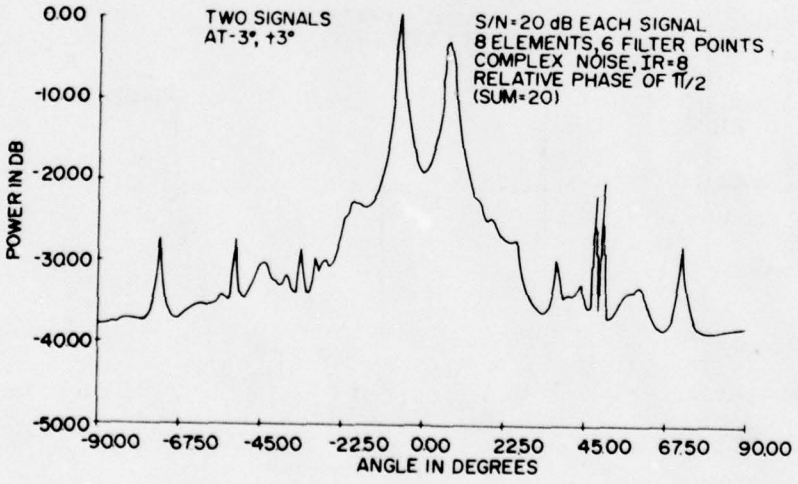

Fig. 20 — Two signals (relative phase of $\pi/2$)

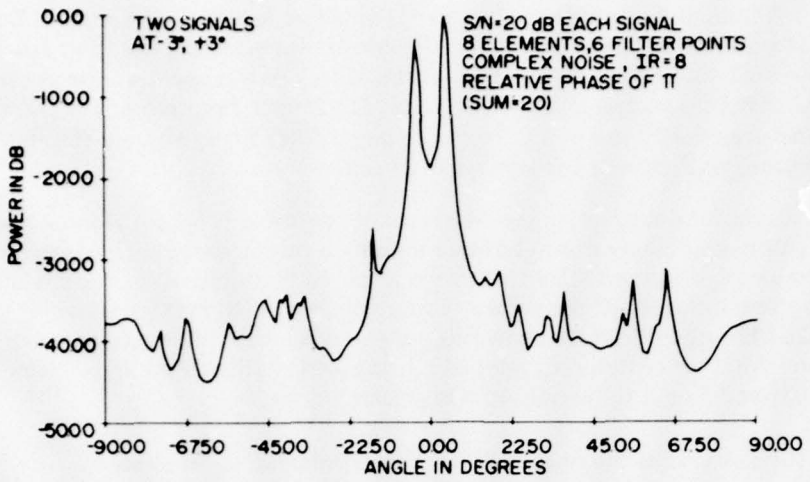

Fig. 21 — Two signals (relative phase of π)

Examples of phase distortion are noted for phases π and $\pi/2$, which are thought to be most troublesome.

One type of averaging, postprocessor integration, is shown to be most effective in providing stability in the computed MESA patterns and in substantially improving signal detection. It is likely that preprocessor integration is equally effective, and may be preferable to postprocessor integration when computational time is considered.

OPTIMAL FILTER SIZE

The size N (number of filter coefficients) of a MESA filter is constrained to be at least one less than the number of data samples M, i.e.,

$$N \leqslant M - 1,$$

so that at least one data sample which is not convolved with the filter coefficients is available for estimating the prediction error. The lower bound on N is dependent upon the total number of spectral parameters, since some minimal number of filter coefficients is required to accurately represent all spectral component parameters such as amplitude, frequency, and phase. For instance, if there are P spectral components, all with the same relative phase, then N is constrained as follows:

$$2P \leqslant N \leqslant M - 1, \tag{26}$$

where $2P$ represents the total number of spectral parameters.

While N is bounded, the actual filter size is optional within the bounds of Eq. (26). Anderson [18] and others have noted that the criteria for selecting the filter size depend upon the intended application or function of the MESA power spectra. For in using MESA, it is observed that the spectral characteristics of MESA are a function of the filter size. Both resolution and peak height are improved at the larger filter sizes, whereas stability and accuracy sometimes are better at the smaller filter sizes.

Some criteria for determining the filter size are required if MESA is to be used in a completely automated manner to determine unknown power spectra. One criterion, which is representative of two MESA characteristics, is the output S/η. Peak height and resolution are two interrelated properties that are optimal with maximization of the output S/η. King [20] has noted that maximization of the output S/η at a spectral peak is a reliable criterion. Another criterion developed by Akaike [21] has been investigated by Ulrych and Bishop [8] and found to be only partially satisfactory.

King [20] noted that the output S/η at a spectral peak ω_0 is given by

$$(S/\eta)_{\omega_0} = \frac{P(\omega_0)}{P_N}, \tag{27}$$

where the power spectra are evaluated at the spectral peak ω_0. With use of the power spectra expression (Eq. 6),

$$\left(\frac{S}{\eta}\right)_{\omega_0} = \frac{1}{\Gamma_N^2(\omega_0)}, \tag{28}$$

where

$$\Gamma_N^2(\omega_0) = W \left| 1 + \sum_{n=1}^{N} \gamma_n e^{i\omega_0 n(\Delta t)} \right|^2 . \tag{29}$$

A maximum $(S/\eta)_{\omega_0}$ requires that $\Gamma_N(\omega_0)$ be a minimum. Therefore, an optimal filter size is the filter size (N_0) that minimizes $\Gamma_N(\omega_0)$.

If the maximum S/η is a criterion for determining the filter size, then the MESA properties of accuracy and stability are not optimized, and remain as inherent MESA characteristics. Both accuracy and stability (under varying noise fields) have been satisfactory with use of a maximum S/η output. However, when signal relative phase is nonzero, spectral peaks of the computed power spectra are often instable. Sometimes, averaging of such computed spectra appears to restore the stability. Examples of MESA antenna patterns of phase-shifted signals are provided in the previous section.

Of course, maximization of the output S/η at each spectral peak requires that the peak locations ω_0 be known. The peak locations may be determined by solving for the roots of the function $\Gamma_N(\omega)$ at a stable and accurate low-order filter size. Knowledge of the peak locations is also most helpful in accurately representing computed power spectra.

An example of the value of maximizing the output $(S/\eta)_{\omega_0}$ is given in Fig. 22(a-g), where the MESA wavenumber spectra are computed for a signal located at 0° (broadside to the antenna). The antenna has eight elements and the input S/η is 0 dB per element. The MESA power spectra are shown computed for all possible filter sizes $2 \leq N \leq 7$ in Fig. 22(a-f).

A familiar problem with MESA, line splitting occurs at the larger filter sizes $5 \leq N \leq 7$. At the lower filter sizes $2 \leq N \leq 4$, the power spectra having the best resolution and greatest peak height occur at the filter size $N = 4$, Fig. 22(c). The filter size $N = 4$ is also the size determined by maximizing the output $(S/\eta)_{\omega_0}$, and the optimal power spectra for $N = 4$ are shown in Fig. 22(g). Of the six possible filter sizes, the power spectra for $N = 4$ are clearly those with the best resolution and peak height. Maximization of the output $(S/\eta)_{\omega_0}$ also serves to avoid such problems as peak splitting as observed with the example given.

CONCLUSIONS

Examples of MESA antenna patterns presented in this report are an improvement over conventional phased-array antenna patterns. Several direct comparisons illustrate the improved resolution and side-peak suppression that are characteristic of MESA. However, it should be emphasized that these results were obtained from computer simulation modelling of the antenna elements and the sources. The simulations did not include degrading effects such as antenna errors, signal scintillations, etc., so that it is not appropriate to assume that these remarkable resolution characteristics of MESA will hold under real-life conditions.

The best means of applying MESA to actual radar signals has not been established. Apparently some form of integration (or averaging) is necessary at some point within the MESA algorithm in order to gain stability in the computed antenna patterns. Postintegration (or pattern averaging) demonstrated in this report is one method for obtaining pattern stability. However, stability may also be obtained by averaging the elements of the covariance matrix, the prediction errors, or the prediction filter coefficients.

While MESA appears to be a useful method for obtaining improved antenna patterns, it remains to qualify these improvements and to establish the appropriate applications of MESA to radar problems through further analytical and experimental investigation.

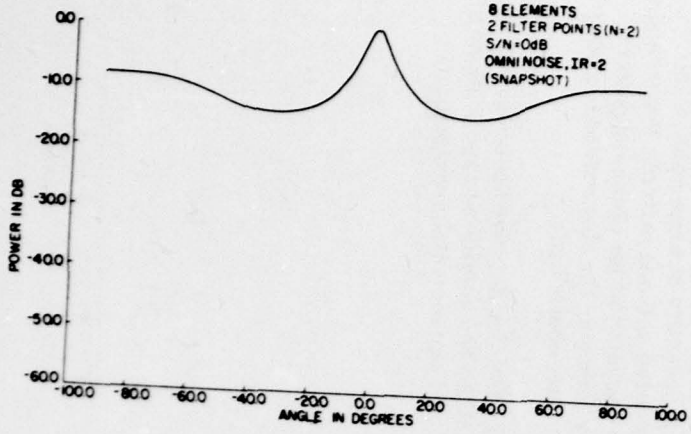

(a) $N = 2$

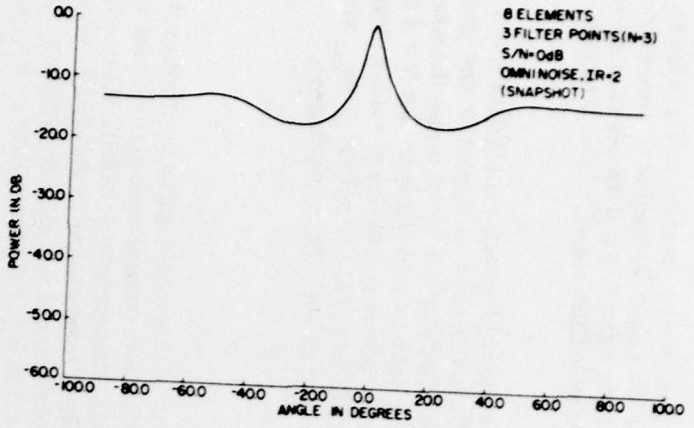

(b) $N = 3$

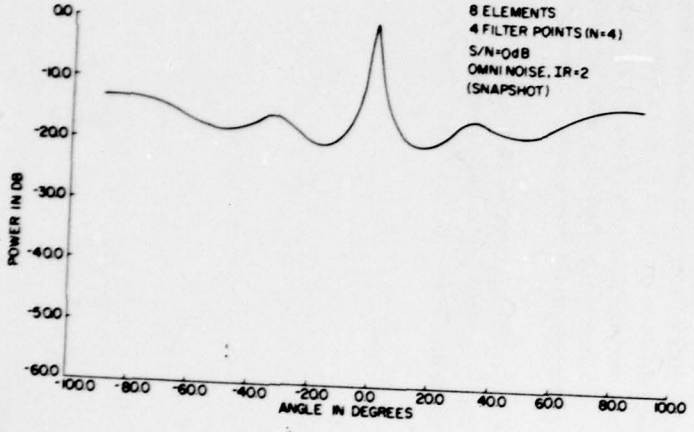

(c) $N = 4$

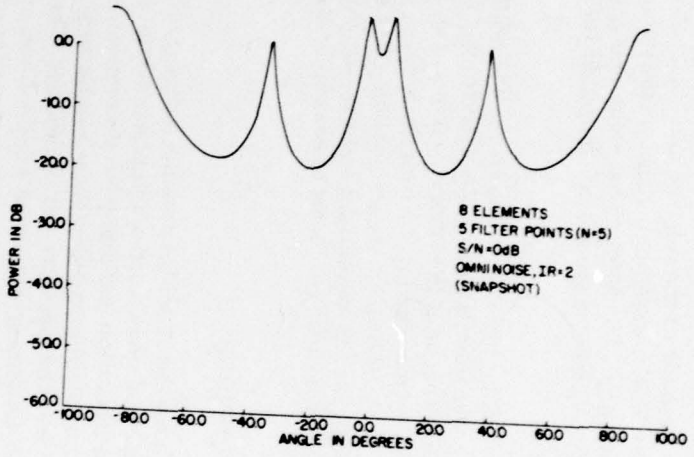

(d) $N = 5$

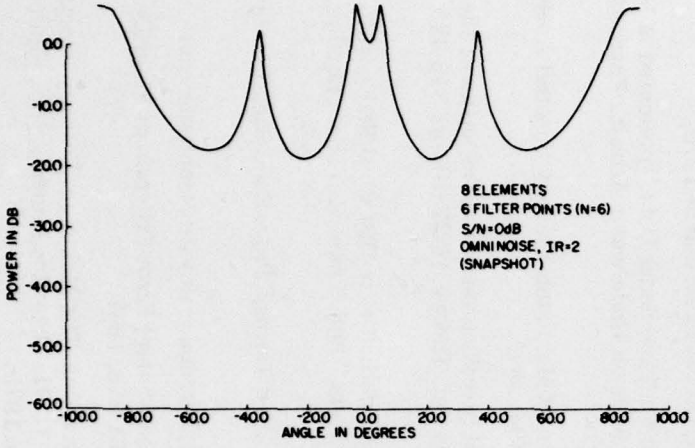

(e) $N = 6$

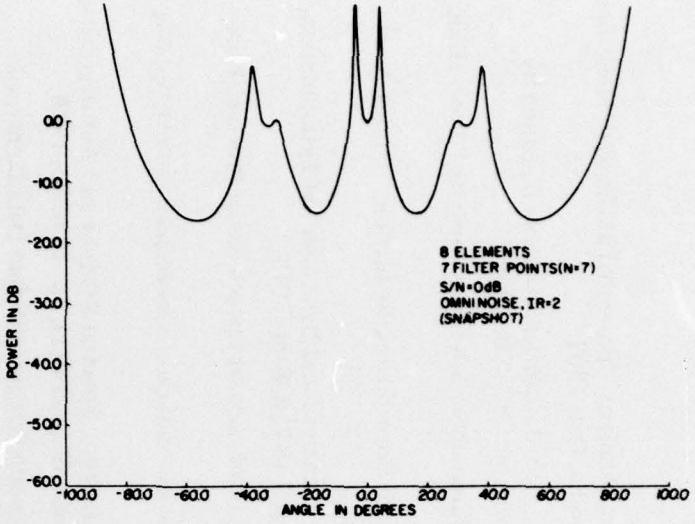

(f) $N = 7$

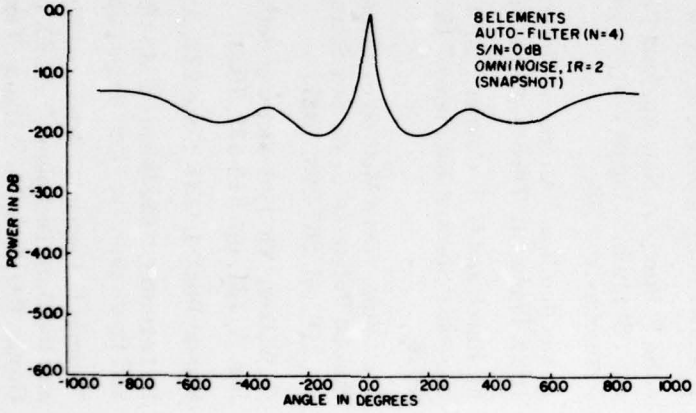

(g) Auto-filter

Fig. 22 — One signal at 0°

REFERENCES

1. John P. Burg, "Maximum Entropy Spectral Analysis," presented at the 37th Meet. Soc. Explor. Geophys., Oklahoma City, Oklahoma, Oct. 1967.
2. E. Parzen, "Multiple Time Series Modeling," in *Multivariate Analysis-II*, edited by P.R. Kirshnaiah, Academic Press, New York, pp. 389-409, 1969.
3. J. Capon, "High-Resolution Frequency-Wavenumber Spectrum Analysis," Proc. IEEE, 57, pp. 1408-1418, 1969.
4. R.W. Gerchberg, "Super Resolution through Error Energy Reduction," Optica Acta, 21 (9), pp. 709-720, 1974.
5. A. Papoulis, "A New Algorithm in Spectral Analysis and Band Limited Extrapolation," IEEE Trans. Circuits Syst., CAS-22 (9), pp. 735-742, Sept. 1975.
6. Gray, "G-Spectral Estimation," IEEE Int. Conf. Acoust Speech Signal Process., Hartford, Connecticut, May 1977.
7. R.T. Lacoss, "Data Adaptive Spectral Analysis Methods," Geophysics, 36 (4), pp. 661-675, Aug. 1971.
8. T.J. Ulrych and T.N. Bishop, "Maximum Entropy Spectral Analysis and Autoregressive Decomposition," Reviews of Geophys. Space Phys., 13 (1), pp. 183-200, 1975.
9. A.H. Nuttall, "Spectral Analysis of a Univariate Process with Bad Data Points, via Maximum Entropy and Linear Predictive Techniques," NUSC Tech. Rpt. 5303, Naval Underwater Systems Center, New London, Connecticut. March 1976.
10. John P. Burg, "A New Analysis Technique for Time Series Data," presented at NATO Adv. Study Inst. Signal Process. with Emphasis on Underwater Acoust., Enschede, Netherlands, 1968.
11. A. van den Bos, "Alternative Interpretation of Maximum Entropy Spectral Analysis," IEEE Trans. Inf. Theory, IT-17, pp. 493-494, 1971.
12. M. Kaveh and G.R. Cooper, "An Empirical Investigation of the Properties of the Autoregressive Spectral Estimator," IEEE Trans. Inf. Theory, IT-22 (3), pp. 313-323, May 1976.
13. G.U. Yule, "On a Method of Investigating Periodicities in Disturbed Series with Special Reference to Wolfers Sunspot Numbers," Phil. Trans. Roy. Soc. London, Ser. A., 226, pp. 267-298, 1927.
14. G. Walker, "On Periodicity in Series of Related Terms," Proc. Roy. Soc., London, Ser. A, 131, pp. 518-532, 1931.
15. Marvin Blizard, ONR Code 222, Arlington, Virginia — private communication.
16. H. Levinson, "The Wiener RMS (Root Mean Square) Error Criterion in Filter Design and Prediction," J. Math. Phys., 25, pp. 261-278, 1947.
17. Thomas E. Barnard, "Advanced Signal Processing. The Maximum Entropy Spectrum and the Burg Technique," ALEX (03)-TR-75-01. Texas Instruments, Inc., Equipment Group, P.O. Box 6015, Dallas, Texas, June 1975.

18. N. Andersen, "On the Calculation of Filter Coefficients for Maximum Entropy Spectral Analysis," Geophysics, 39 (1), pp. 69-72 Feb. 1974.

19. P.F. Fougere, E.J. Zawalick, and H.R. Radoski, "Spontaneous Line Splitting in Maximum Entropy Power Spectrum Analysis," Phys Earth and Planet. Inter., 12, pp. 201-207, 1976.

20. William R. King, "Some Effects of Noise Upon Maximum Entropy Spectral Analysis", NRL Memo Rpt. 3645, Nov. 1977.

21. H. Akaike, "A New Look at the Statistical Model Identification," IEEE Trans. Automat. Control, AC-19, pp. 716-723, 1974.

APPENDIX A
WIENER PREDICTION FILTER

PREDICTION FILTER

Consider a signal $x(t)$ with a waveform known only over the time interval $(0,T)$. The waveform may be predicted (or estimated) for points outside the window $(0,T)$ by using the prediction filter in a convolution with the known signal $x(t)$ as follows (suggested by Wiener*):

$$\hat{x}(t) = \int_0^T a(\tau)\, x\,(t - \tau)\, d\tau, \tag{A1}$$

where $\hat{x}(t)$ is the predicted signal and $a(\tau)$ is the impulse response of the prediction filter.

If the signal has been adequately sampled within the time interval $(0,T)$ such that

$$\Delta t \leqslant \frac{1}{2f}, \frac{(M-1)}{T} \leqslant 2f,$$

for a sampling interval Δt, M data samples, and signal frequency f, then the discrete convolution may be employed as follows:

$$\hat{x}_k = \sum_{n=1}^{N} a_n\, x_{k-n}\,, \quad N < M, \tag{A2}$$

where the summation is taken over N filter coefficients, N being less than the number of data samples.

PREDICTION ERROR FILTER

An error ϵ_k may be defined for the known set of data samples by

$$\begin{aligned} \epsilon_k &= x_k - \hat{x}_k \\ &= x_k - \sum_{n=1}^{N} a_n x_{k-n} \\ &= \sum_{n=0}^{N} \gamma_n x_{k-n} \end{aligned} \tag{A3}$$

*N. Wiener, *Extrapolation, Interpolation, and Smoothing of Stationary Time Series*, John Wiley and Sons, Inc., New York, N.Y. 1949.

for

$$\gamma_0 = 1, n = 0,$$

$$\gamma_n = -a_n, n > 0,$$

where γ_n is the nth prediction error filter coefficient.

The squared error is expressed as follows:

$$\epsilon_k^2 = \sum_{m=0}^{N} \sum_{n=0}^{N} \gamma_n \gamma_m x_{k-n} x_{k-m}^* . \tag{A4}$$

Since $\gamma_0 = 1$, there are N remaining unknown prediction error coefficients. These N coefficients may be determined by minimizing the total mean squared error E_N which is defined by

$$E_N = \frac{1}{M+1} \sum_{k=-M}^{M} \epsilon_k^2 . \tag{A5}$$

The summation is taken over all errors possible to compute in a forward prediction within the data window defined by $N + 1$ data samples. The incorporation of Eq. (A4) into Eq. (A5) results in the following equation:

$$E_N = \frac{1}{N+1} \sum_{k=-M}^{M} \sum_{m=0}^{N} \sum_{n=0}^{N} \gamma_n \gamma_m x_{k-n} x_{k-m}^*$$

$$= \sum_{m=0}^{N} \sum_{n=0}^{N} \gamma_n \gamma_m \frac{1}{M+1} \sum_{k=-M}^{M} x_{k-n} x_{k-m}^* \tag{A6}$$

$$E_N = \frac{1}{2} \sum_{m=0}^{N} \sum_{n=0}^{N} r_{m-n} \gamma_n \gamma_m ,$$

where r_{m-n} represents the data set autocorrelation coefficients.

The prediction error coefficients are defined with minimization of the total prediction error as follows:

$$\frac{\partial E_N}{\partial \gamma_k} = \sum_{n=0}^{N} \gamma_n r_{k-n} = 0, \tag{A7}$$

for $k = 1, 2, 3, \ldots N$. The resulting N equations with N unknowns are

$$
\begin{aligned}
k &= 1, \gamma_0 r_1^* + \gamma_1 r_0 + \gamma_2 r_1 + \ldots + \gamma_N r_{N-1} = 0, \\
k &= 2, \gamma_0 r_2^* + \gamma_1 r_1^* + \gamma_2 r_0 + \ldots + \gamma_N r_{N-2} = 0, \\
&\vdots \\
k &= N, \gamma_0 r_N^* + \gamma_1 r_{N-1}^* + \gamma_2 r_{N-2}^* + \ldots + \gamma_N r_0 = 0.
\end{aligned} \tag{A8}
$$

An additional equation which defines E_N results for $k = 0$ where Eq. (A6) is evaluated as follows:

$$E_N = \gamma_0 \sum_{n=0}^{N} \gamma_n r_n \quad \text{for } k = 0, \tag{A9}$$

when it is recalled that $\gamma_0 = 1$.

Burg† has assumed that the mean squared error power E_N, as defined by Eq. (A5) for the time domain, is equivalent to the mean squared error power P_N, which is given by Eq. (8) for the frequency domain. However, King‡ has noted that E_N and P_N are equivalent only when the predicted noise power equals the actual noise power or when the noise power is negligible. It follows that for high signal-to-noise conditions, it may be assumed that

$$P_N = E_N \tag{A10}$$

and P_N may be evaluated as follows:

$$P_N = \sum_{n=0}^{N} \gamma_n r_n \text{ for } k = 0, \tag{A11}$$

or

$$\gamma_0 r_0 + \gamma_1 + \gamma_2 r_2 + \ldots \gamma_N r_N = P_N. \tag{A12}$$

If Eq. (A12) is combined with the set of equations (A8), the resulting set of equations may be expressed in matrix formulation as follows:

$$
\begin{bmatrix}
r_0 r_1 r_2 r_3 \cdots r_N \\
r_1^* r_0 r_1 r_2 \cdots r_{N-1} \\
r_2^* r_1^* r_0 r_1 \cdots r_{N-2} \\
\cdot \\
\cdot \\
\cdot \\
r_N^* r_{N-1}^* r_{N-2}^* r_{N-3}^* \cdots r_0
\end{bmatrix}
\cdot
\begin{bmatrix}
\gamma_0 \\ \gamma_1 \\ \gamma_2 \\ \cdot \\ \cdot \\ \cdot \\ \gamma_N
\end{bmatrix}
=
\begin{bmatrix}
P_N \\ 0 \\ 0 \\ \cdot \\ \cdot \\ \cdot \\ 0
\end{bmatrix}
\tag{A13}
$$

†John P. Burg, "Maximum Entropy Spectral Analysis," presented at the 37th Meet. Soc. Explor. Geophys., Oklahoma City, Oklahoma, Oct. 1967.

‡William R. King, "Some Effects of Noise Upon Maximum Entropy Spectral Analysis," NRL Memorandum Report 3645, Nov. 1977.

APPENDIX B

THE BURG TECHNIQUE

Burg† has proposed a method for computing a set of $N + 1$ prediction error filter coefficients as a function of a known set of N coefficients using the Levinson recursion equation

$$\gamma_k^{N+1} = \gamma_k^N + \gamma_{N+1}^{N+1} \left(\gamma_{N-k+2}^N \right)^* , \tag{B1}$$

where the only unknown in Eq. (B1) is the last coefficient γ_{N+1}^{N+1} of the new set. Burg suggested that the unknown coefficient γ_{N+1}^{N+1} be obtained in a least-square error analysis that incorporates both the forward and backward prediction of the kth point as follows:

$$\vec{X}_k = \sum_{n=1}^{N} a_n^N x_{k-n} , \tag{B2}$$

$$\overleftarrow{X}_k = \sum_{n=1}^{N} a_n^N x_{k+n} , \tag{B3}$$

where the forward prediction $\vec{X}_k$ and the backward prediction $\overleftarrow{X}_k$ are expressed as discrete convolutions of the prediction filter set a_n^N (of size N) with the set of $N + 1$ data samples.

It follows that corresponding forward and backward prediction errors, denoted by α_k^N and β_k^N respectively, have the following representations:

$$\alpha_k^N = X_k - \vec{X}_k ,$$

$$\alpha_k^N = \sum_{n=0}^{N} \gamma_n^N x_{k-n} , \qquad \text{for } N + 1 \leq k \leq M , \tag{B4}$$

where M is the number of data samples, and

$$\beta_k = X_k - \overleftarrow{X}_k ,$$

$$\beta_k^N = \sum_{n=0}^{N} \gamma_n^N x_{k+n} , \quad \text{for } 1 \leq k \leq M - N, \tag{B5}$$

where $\gamma_1^{N+1} = 1$ and $\gamma_n^N = -a_n^N$.

†John P. Burg, "A New Analysis Technique for Time Series Data," presented at NATO Adv. Study Inst. Signal Process. with Emphasis on Underwater Acoust., Enschede, Netherlands, 1968.

Barnard† has noted that the forward and backward prediction errors are interrelated through the Levinson recursion relations

$$\alpha_k^{N+1} = \gamma_{N+1}^{N+1} \cdot \beta_{k-N}^{N} + \alpha_k^N , \quad (N+1 \leqslant k \leqslant M), \tag{B6}$$

$$\beta_j^{N+1} = \left(\gamma_{N+1}^{N+1}\right)^* \cdot \alpha_{j+N}^N + \beta_j^N , \quad (1 \leqslant j \leqslant M-N). \tag{B7}$$

The prediction errors may be computed with the Levinson recursion relations given by Eqs. (B6) and (B7) in a bootstrap manner that greatly reduces the number of computations required with use of the matrix formulation given by Eq. (10).

The total mean squared error may be expressed as the sum of the forward and backward mean squared errors as follows:

$$E_N = \frac{1}{2(M-N)} \sum_{k=1}^{M-N} \left[\left(\alpha_{k+N}^N\right)^2 + \left(\beta_k^N\right)^2 \right] \tag{B8}$$

for a filter of size N where $N \leqslant M-1$, with M = number data samples.

In order to use Eqs. (B6) and (B7) as written, the total mean squared error may be expressed for filter size $N+1$ as follows:

$$E_{N+1} = \frac{1}{2(M-N-1)} \sum_{k=1}^{M-N-1} \left[\left(\alpha_{k+N+1}^{N+1}\right)^2 + \left(\beta_k^{N+1}\right)^2 \right] . \tag{B9}$$

Incorporation of the Levinson recursion relations, Eqs. (B6) and (B7), results in the following expression for E_{N+1}:

$$E_{N+1} = \frac{1}{2(M-N-1)} \sum_{k=1}^{M-N-1} \left[\left(\gamma_{N+1}^{N+1} \beta_k^N + \alpha_{k+N}^N\right)^2 + \left(\left(\gamma_{N+1}^{N+1}\right)^* \alpha_{k+N}^N + \beta_k^N\right)^2 \right] \tag{B10}$$

† Thomas E. Barnard, "Advanced Signal Processing. The Maximum Entropy Spectrum and the Burg Technique," ALEX (03)-TR-75-01. Texas Instruments, Inc., Equipment Group, P.O. Box 6015, Dallas, Texas, June 1975.

In order to minimize the mean squared error, the partial derivative with respect to γ_{N+1}^{N+1} (the only unknown filter coefficient) is set equal to zero:

$$\frac{\partial E_{N+1}}{\partial \gamma_{N+1}^{N+1}} = 0$$

$$\frac{1}{2(M-N-1)} \sum_{k=1}^{M-N-1} \left[\left(\gamma_{N+1}^{N+1} \beta_k^N + \alpha_{k+N}^N \right) \beta_k^N + \left(\left(\gamma_{N+1}^{N+1} \right)^* \alpha_{k+N}^N + \beta_k^N \right) \alpha_{k+N}^N \right] = 0. \quad \text{(B11)}$$

Equation (B11) may be solved for γ_{N+1}^{N+1} as follows:

$$\gamma_{N+1}^{N+1} = \frac{-2 \sum_{k=1}^{M-N-1} \alpha_{k+N}^N \left(\beta_k^N \right)^*}{\sum_{k=1}^{M-N-1} \left[\left(\alpha_{k+n}^N \right)^2 + \left(\beta_k^N \right)^2 \right]}. \quad \text{(B12)}$$

The new larger set of prediction error coefficients may be evaluated with use of the recursion relation, Eq. (B1), and Eq. (B12), which greatly reduces the number of computations required of the matrix formulation given by Eq. (10).

DEPARTMENT OF THE NAVY

NAVAL RESEARCH LABORATORY
Washington, D.C. 20375

OFFICIAL BUSINESS
PENALTY FOR PRIVATE USE, $300
THIRD CLASS MAIL

POSTAGE AND FEES PAID
DEPARTMENT OF THE NAVY
DoD-316
THIRD CLASS MAIL